Bull. Disas. Prev. Res. Inst., Kyoto Univ., Vol. 39, Part 3, No. 341, September, 1989

Damage Assessment of Steel Elements for Seismic Reliability Estimation of Structural Systems

By Ulrich BOURGUND, Satoshi IWAI, Hiroyuki KAMEDA and Taijiro NONAKA

(Manuscript received July 3, 1989)

Abstract

Based on experimental investigations using steel plate elements subjected to cyclic uniaxial loading, a continuous damage and/or deteriorating process is examined. In order to describe intermediate as well as ultimate damage states, energy related criteria for different types of failure modes are suggested. Pure tensile and compressive/tensile bending damage could be distinguished clearly on the basis of plastic deformation properties. The respective dissipated energies of the investigated specimens are calculated by use of an axial load-displacement coordinate system whose origin is adaptively shifted so as to divide the regions of the two damage contributions. The combination of the considered damage contributions to one single damage index is performed by set theory operations. Calculated damage indices could be correlated fairly well to actual physical damage observed during the experimental investigations.

1. Introduction

Efficient and practical damage assessment of structural systems undergoing seismic excitation is of great importance, since the economic effects of earthquake damage in certain areas can be quite significant. Therefore, it is essential to assess the expected physical damage level for elements of structural systems, which might finally enable improved general reliability/risk estimation. The investigations in this series of study are focused on the very low-cycle fatigue range (5–20 cycles of repetition) because of its importance with respect to earthquake engineering damage assessment. The damage assessment at the present step of investigation is confined to structural steel elements under cyclic axial loading which can be considered to reflect the behavior of braced members and/or their components. All developments are based on experimental investigations in order to verify a damage model as close to the actual physical behavior as possible. Special attention is given to different types of failure modes, e.g. failure due to: a) compression and bending, b) tension and bending, c) pure tension. The existence of different failure patterns can be clearly observed by investigating the unsymmetric complex hysteretic behavior of the specimen. Under larger tensile axial force, load-carrying capacity of any specimen is only related to its respective cross-section; whereas a larger compressive force induces buckling, and hence the compressive strength depends on slenderness, which involves cross-sectional properties

as well as its length. Therefore, the effects from these completely different types of structural behavior have to be considered separately with respect to damage effects and damage evaluation. Due to the presence of instability effects, the damage modeling refers to structural damage rather than to material damage.

The present investigation includes the inelastic post-buckling range of structural members. This range in general has no influence on structural design considerations, but with respect to the load redistribution process in a structural system and strength reversals due to seismic loading, it is rather likely that buckled members will undergo stress reversals. Therefore, the present investigation has considerable importance concerning structural reliability estimation procedures. Furthermore, since optimum design may give less damage concentration, our investigation might lead to improved optimum design considerations.

2. Outline of Experimental Study[1)]

The specimen used in this experiment is shown in **Fig. 1.** A simple but fundamental rectangular cross-section was selected as reference for future, more complicated sections. Each test was performed up to complete failure of the specimen, in order to observe the structural failure phenomena in detail. The middle part of the specimen has a weaker cross-section (see **Fig. 1**), with the same area for all the specimens, to simulate local buckling behavior of thin plate elements of structural members. At both ends, pin-supported condition was selected. A total of nine specimens were designed with a medium range of slenderness ratios which may cause either

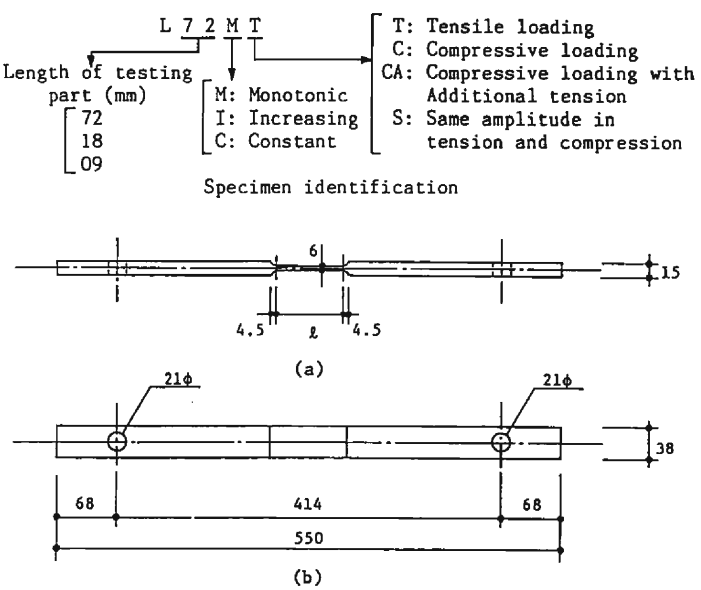

Fig. 1. Test Specimen (length in mm).

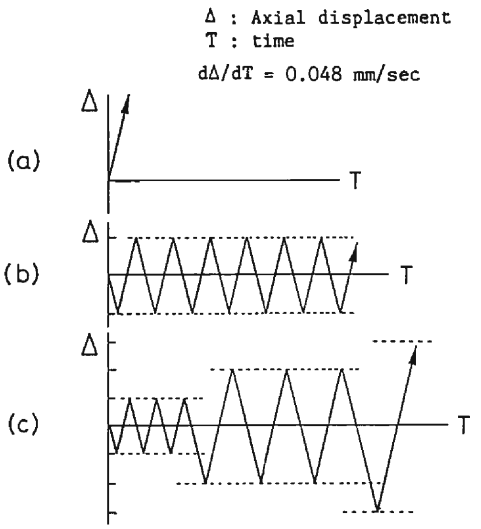

Fig. 2. Loading Patterns.

elastic or inelastic buckling.

Load was applied to each specimen with one of the controlled uniaxial displacement patterns, as shown in **Fig. 2**. The specimens' behavior was monitored by strain gages and displacement meters. The general behavior of the specimen for the first and second cycle at two different amplitude levels in terms of axial load (P) and axial displacement (Δ) as well as mid-height deflection (V) is shown in **Figs. 3(a)** and **3(b)**, revealing clearly the unsymmetric shape of the hysteresis loop. The shapes of the theoretical deflection curve are shown in **Fig. 3(c)** as well as the directions of the load application. The encircled numerals indicate the sequence of load-displacement states[2].

Since tracing the plastic deformation is extremely difficult by strain gages only, this range has been monitored especially by displacement meters. In order to relate real physical damage such as cracks to load-deformation curves, the behavior of all test specimens was recorded in video tapes, which helped to detect the onset of failure.

Table 1 shows all specimens so far tested. From **Table 1** it can be noted that the specimen name contains the length of weak sectional part (l=72, 18, 9 mm). For the following discussion, L72-series is referred to as specimens No. 1, 2, 3, 4, L18-series as No. 7, 8, 9 and L09-series as No. 10, 11, respectively. Since reference values with respect to strength drop and plastification (pure tensile plastification, compressive bending plastification) as well as deformation energy seem to be necessary, monotonic loading tests (Specimens No. 2 and No. 11) have been performed. Type of failure and amplitude of displacement as well as the respective number of cycles are also displayed in **Table 1**. For further details of the experimental investigations the reader is referred to [1].

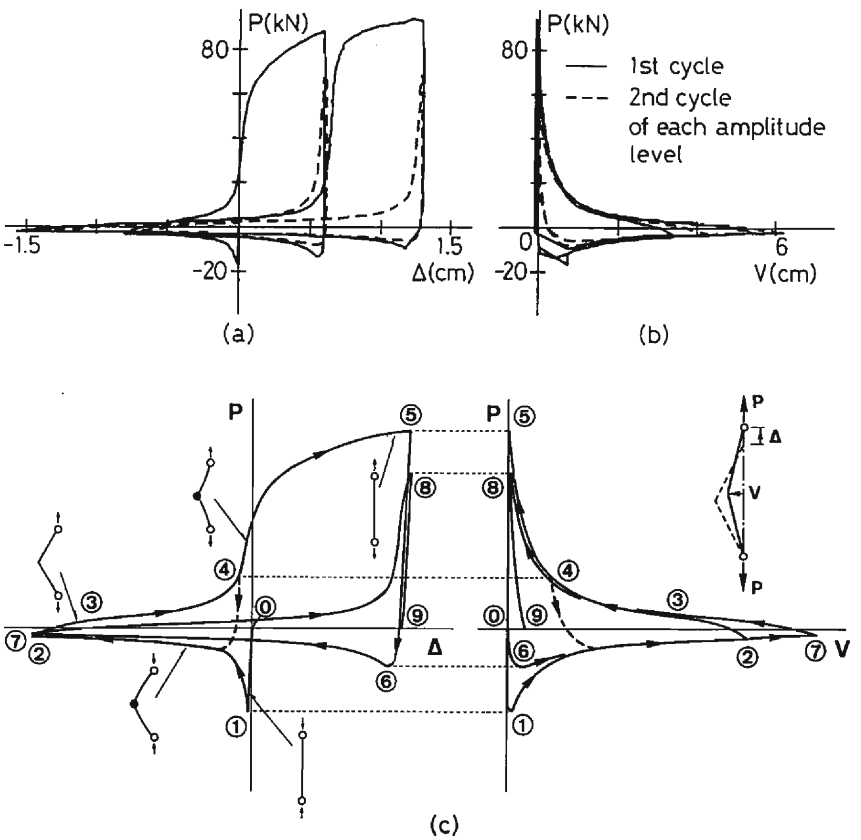

Fig. 3 (a) Axial Load vs. Displacement Relation. (b) Axial Load vs. Deflection Relation. (c) Load-Displacement States of Specimen.

3. Review of Parameters for Damage Assessment

Numerous approaches to damage assessment have been suggested in recent years which reflect somehow the importance and necessity of damage estimation. The general principles of the most important models are discussed in this section in order to provide some basic aspects on alternative methods. For more exhaustive literature survey and further discussion, the reader is referred to the papers listed in the references [2),3)].

One of the most frequently used approaches for damage assessment is performed in terms of ductility or ductility ratios. Ductility indicates the relation between actual deformation and yield deformation. The ductility demand—reflecting a response quantity due to applied loading pattern—is usually compared with ductility capacity which indicates the maximum ductility close to failure. Ductility can be defined for any deformation quantity like system deformation (global ductility) or curvature of any structural element (local ductility). One drawback in the use of ductility as a damage parameter seems to be the fact that both recoverable and permanent

deformation quantities are contained. A possibility to overcome the disadvantage of included recoverable deformation is the application of plasticity ratio. Plasticity ratio in this context denotes the relationship of residual plastic deformation at zero loading and elastic deformation at yield limit. However, it might be rather difficult to use both ductility and plasticity ratios for cumulative damage assessment.

A different approach can be performed in applying stiffness ratios as the relation between initial stiffness and secant stiffness at maximum possible deformation. Stiffness ratios are rather attractive since they combine information about strength and deformation. Similar to ductility considerations, stiffness ratios are rather difficult to apply to damage accumulation and furthermore—especially related to the present investigations—stiffness cannot be defined uniquely in behavior of certain structural specimens and type of loading.

Continuum damage mechanics approaches (for example Kachanov[4]) also have been considered during these investigations. Especially the mixed type of influences—structural parameters like slenderness ratio and material properties—on damage development make these approaches less attractive since they are usually confined to the microscale range related to material properties only. Furthermore, it should be noted that continuum damage mechanics requires microscale direct (observation of micrographic pictures) or non-direct measurements (variation of moduli of elasticity) to verify the damage evaluation. Since this type of investigation is much localized, it is still not clear how to assess the degree of damage of a cross-section or structural element.

The investigation of energy behavior—dissipated energy or strain energy (work)—seems to be one of the most general approaches to damage estimation, since unique definitions for different types of specimens and of loading patterns can be formulated, combining both strength and deformation effects. Unfortunately, energy dissipation capacity is not constant but dependent on loading history and failure mode. But without loss of generality it can be stated that dissipated energy per loading cycle decreases with increased damage. A physical meaningful verification of energy dissipation has been suggested by Koenig[5] and Meyer[6], distinguishing between primary and secondary cycle energy. A primary cycle is defined as the first loading cycle on each amplitude level, while all the following cycles at the same level are considered as secondary cycles. Physically this separation reflects the assumption that a major contribution or initiation of damage is due to the first cycle at each amplitude level, while all the following cycles cause cumulative damage. Furthermore, this way of separating different contributions means that damage is strongly related to maximum values, e.g. maximum deformation and maximum strain energy or dissipated energy.

Since dieffrent types of failure modes will occur in this investigation, different damage modes have to be combined to assess the overall damage level. The interaction of different damage modes has seldom been discussed in the present literature in spite of it being a topic of importance.

The main drawbacks in many existing damage parameters are related to the lack of reflecting the loading history and the assumption of linear damage accumulation

such as Miner's Rule. Linear damage accumulation might be true in special cases. However, neglecting the loading history may lead to considerable errors in damage estimation. Energy related damage criteria seem to be most attractive in this situation since they reflect loading history as well as the type of failure mode.

4. General Remarks on Damage Modeling

One of the most important topics related to damage assessment is concerned with the definition of failure. In the present investigation, rupture is always referred to as complete failure, while other investigators sometimes define failure in terms of a predefined strength drop. The former has been selected here since one of the topics under investigation is the examination of the details of damage, tracing it up to complete rupture, where complete rupture might serve as an important boundary state. Strength drop related failure definitions have to be considered as misleading in many cases, since cyclic loading pattern might result in considerable strength recovery as displayed in **Fig. 4**. The strength development in **Fig. 4** is measured at specimen No. 1 where a symmetric type of loading pattern (equal amplitude in tension and compression) with increased amplitudes is applied. It is clear that at the first ampli-

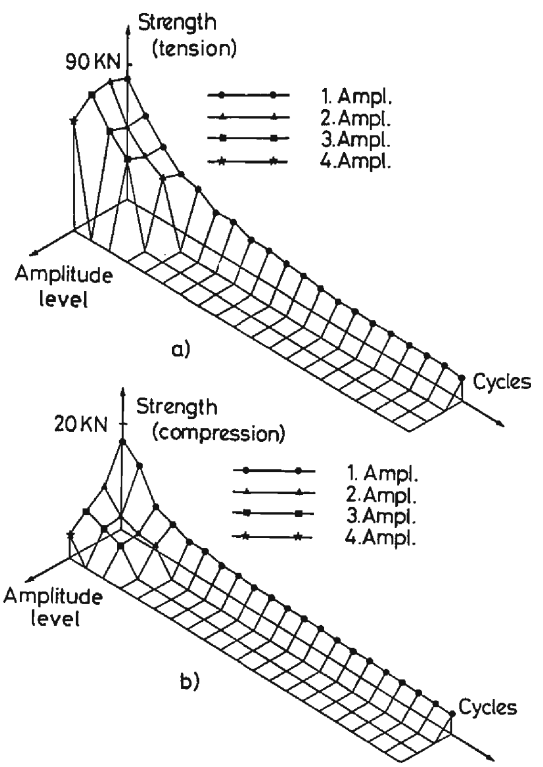

Fig. 4. Strength Deterioration in Tensile and Compressive Loading (Specimen No. 1).

tude level, both tensile (**Fig. 4(a)**) and compressive (**Fig. 4(b)**) strength decreases continuously until loading at an increased amplitude level occurs. In this situation, tensile and compressive strength recovers. Due to stability effects the compressive strength recovers considerably less than the tensile strength. Since specimen No. 1 failed in pure tensile fracture, it is obvious that the peak values of tensile strength at the first cycle of each amplitude level display a similar curve as usually obtained for the strain-hardening and deteriorating part of a monotonic tensile loading curve. A comparison with results from specimen No. 2 revealed that the monotonic tensile load-displacement curve yields the envelope of the respective cyclic load-deformation curve.

Since the present investigation is focused on the very low-cycle fatigue (damage) range, damage development is strongly related to plastification. Therefore, no damage is assumed as long as no plastification occurs in any cross-section. The specimens were designed to undergo buckling elastically or inelastically. Nevertheless in the post-buckling range, plastification takes place due to large deformations and *P*-delta effects (second-order contributions). This part of the load-displacement curve is hereafter referred to as **compressive bending range**. After unloading at peak displacement in the post-buckling range, reverse plastification—due to reversed *P*-delta effects—at the extreme fibers of the weaker cross-section can be observed (see **Fig. 3(c)**). For convenience in discussion, this range is defined as **tensile bending range**. When the specimen becomes straight again, tensile plastification will result in elongation of the specimen. This part is referred to as **pure tensile loading range**. It should be noted that this range occurs only at the first cycle of each amplitude level which is discussed in more detail in **section 5.2**. In the following compressive re-loading, it might be interesting to note that tensile elongation (plastification) cannot be reversed since buckling occurs due to the slenderness of the specimen.

From the above considerations of the specimens' behavior it can be concluded that pure tensile failure (damage) and compressive/tensile bending failure have to be clearly separated. The interaction between these types of failure modes is difficult to estimate, but it seems to be obvious that the first type of plastification (compressive bending or pure tensile plastification) will at least initiate certain types of microcracks which will have some influence on the failure pattern.

5. Energy Considerations

5.1 Discussion of Energy Dissipation Behavior

If energy dissipation is considered as irreversible energy transformation in terms of thermodynamics, this quantity might provide some information about damage development. In order to provide more insight into energy dissipation behavior, specimen No. 1 was investigated in more detail with respect to energy contributions from different cycles (**Fig. 5**) where (.) provides the cycle number. In this investigation one cycle is defined with reference to applied loading, starting at zero, undergoing

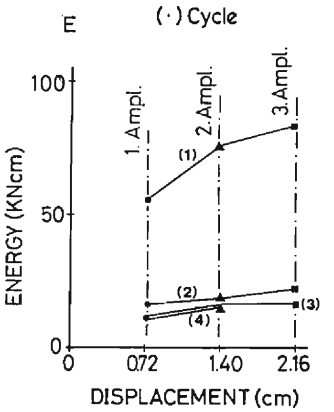

Fig. 5. Energy Contributions from Different Cycles (Specimen No. 1).

load reversal and returning to zero. Clearly it can be noticed that the energy contribution from the first cycle at each amplitude level is dominant to all other following cycles. This fact seems to justify the concept of primary and secondary cycles as mentioned earlier. Furthermore, **Fig.** 5 reveals that there is a strong dependence between energy dissipation and displacement level (the first cycle at each amplitude level); therefore, these quantities can not be treated independently. In order to provide some comparison between all tested specimens and the respective energetic behavior, normalized dissipated energies are displayed in **Fig. 6**. The normalizing value E_o is calculated as the maximum capacity of elastic strain energy of the weak cross-sectional part. Numbering of the curves refers to the specimen numbers given in **Table 1**, as well as the type of failure observed, CF (compressive failure), TF (tensile failure) and NF (no failure). The major energy contribution from the first cycle at each amplitude level for specimen No. 1 can be noticed once again, but as the number of cycles increases the cumulative energy effects gain greater importance.

Total energy dissipation is clearly different even among specimens of the same series (for example No. 10 and No. 11) and seems to be strongly related to loading history. The observed damage development detected during testing of each specimen is also given in the respective energy dissipation curves. In some specimens, the damage process occurred rather slowly, wherein small visible cracks at the flexural-tension side (VCT), visible cracks at the flexural-compressive side (VCC), larger major cracks (MC) and considerable increased major cracks (IMC) just before complete failure could be observed. Increased major cracking might be already considered as complete failure (structural failure), since at this stage of damage a large area of the cross-section is disintegrated. It is interesting to note that specimens No. 1 and No. 4, after completing the first cycle, dissipate energy for the following three cycles in a proportional way. With respect to energy dissipation the considerably larger amplitude of specimen No. 4 in the first cycle seems to have had only minor effects. Comparing specimen No. 10 with No. 7, similar tendencies in dissipation behavior can be observed, which is due to similar loading characteristics, despite larger strain amplitudes in

specimen No. 7. Furthermore, the energy dissipation curves of specimens No. 8 and No. 9 develop nearly parallelly. While No. 8 is loaded only in a compressive/tensile bending range, No. 9 is additionally loaded to a small degree in the pure tensile range. Slightly beyond the yield limit this pure tensile plastification might be responsible for early small cracks at the flexural-tension side and failure at a lower dissipated energy level and after a smaller number of cycles. The two failure patterns—pure tension failure and compressive/tensile bending failure—usually can be recognized by different behavior at final energy dissipation. Pure tension failure usually coincides with a steep increase of dissipated energy (No. 1, No. 4), while compressive/tensile bending failure in most cases displays decreasing total energy dissipation behavior before complete failure (No. 8, No. 10).

5.2 Energy Separation Based on Considerations of Plastic Deformation

From the preceding discussion on dissipated energy up to failure it seems to be necessary to investigate in more detail the physical background for different energy contributions. **Fig. 5** shows the significance of the first cycle to energy contribution. This fact can be verified by investigating the relationship of dissipated energy and residual plastic deformation in each cycle (**Figs. 7, 8, 9**). Residual plastic deformation is defined in this investigation as the deformation at zero load. Due to the selected type of specimen and loading history, residual plastic deformation in the compressive/tensile bending range is different in characteristic from residual plastic deformation in the pure tensile range with respect to plastification in the cross-section. It should be noted that the right hand side of the lateral axis in **Figs. 7, 8** and **9** represents the compressive/tensile bending range. Considerable increase in energy dissipation is always related to pure tensile plastification, while compressive/tensile bending plastification increases the dissipated energy somehow proportional to the plastification range even in case of the first cycle at each amplitude level. In order to separate energy contributions—for a better understanding of damage development—it might be useful to recall the specimens' behavior in terms of the plastification process. Starting with compressive loading, after buckling compressive/tensile bending plastification takes place, which is followed by pure tensile plastification (see **Fig. 3**(**c**)). Due to the slenderness of the specimen, buckling will appear immediately in case of compressive re-loading, which means that axial contraction is not present or at least very small. For the following cycles at the same amplitude level this consequently will result—due to the axial displacement controlled loading system—in compressive/tensile bending plastification and re-plastification, since the original specimen is elongated in the first tensile loading. In other words, after the first pure tensile plastification, the P-Δ coordinate system (see **Fig. 10**) has to be shifted in its origin about the value of the maximum axial plastification in order to separate different energy contributions. The center of the coordinate system will remain at this new position as long as no further pure tensile plastification occurs. This way of adaptive shifting provides a clear distinction of energy contributions based on different types of plastification. Furthermore, this approach allows a similar treatment of all different loading patterns applied to the

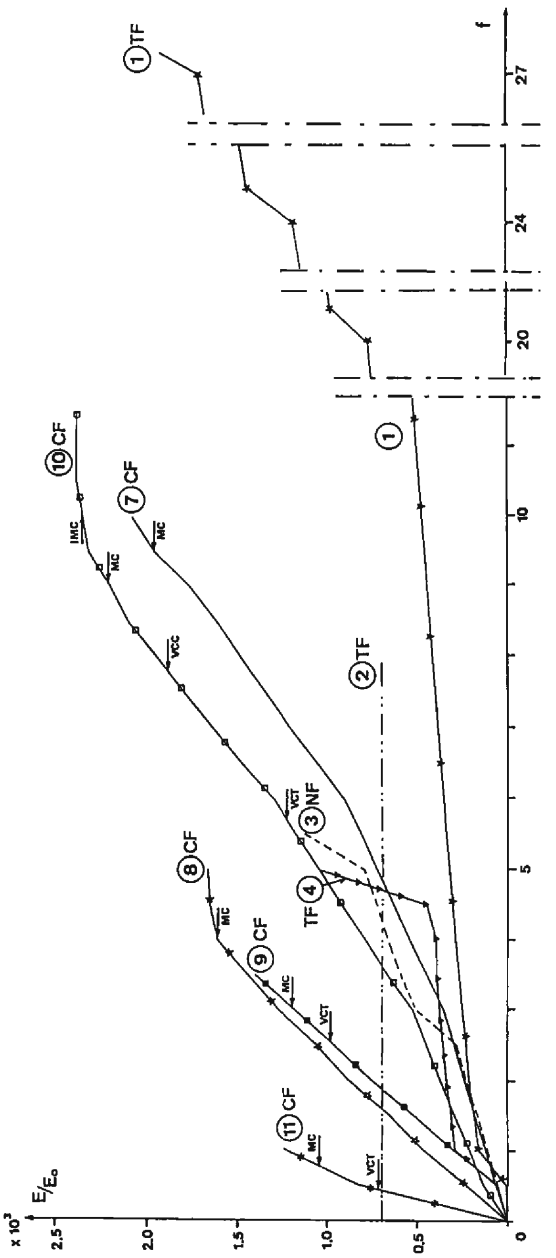

Fig. 6. Development of Normalized Energy Dissipation of All Specimens.

Table 1. Loading Program.

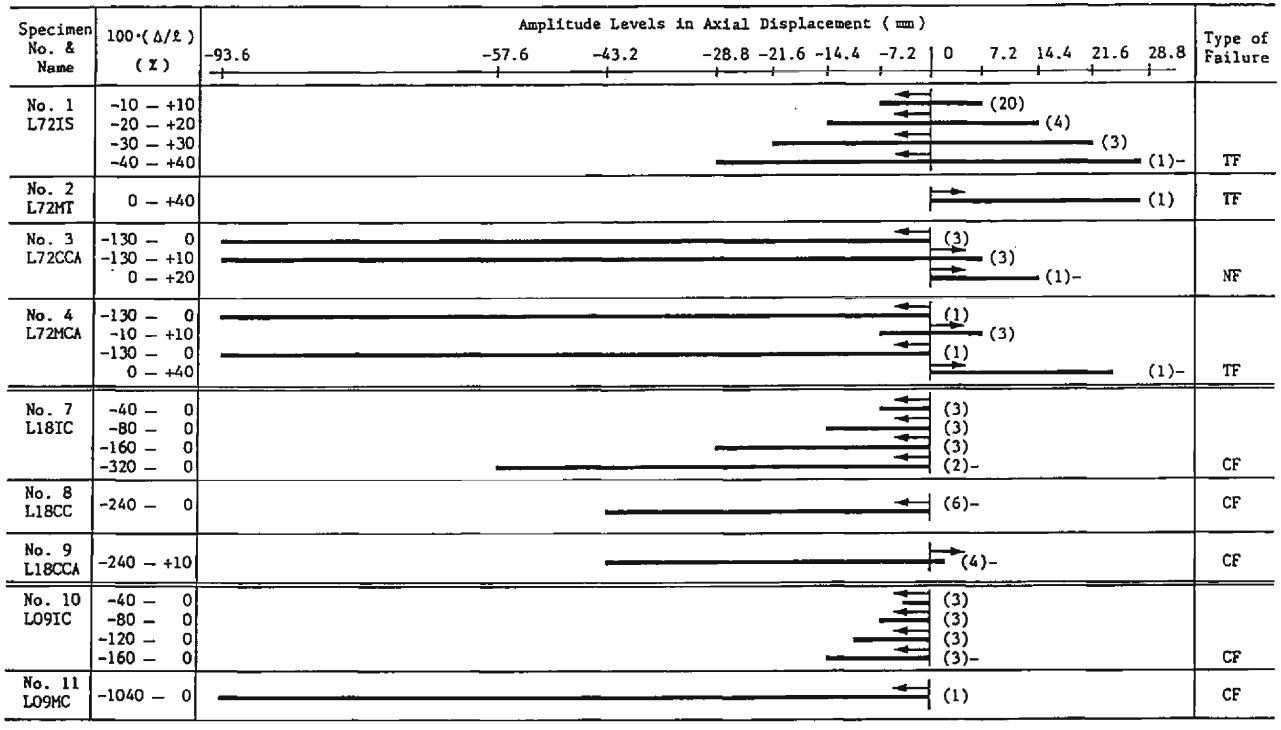

[Notes] ( ): No. of Cycles, - : Last cycle not completed, ◄—: Starting Direction,
TF: Failure in Tension, CF: Failure in Compression, NF: No Failure.

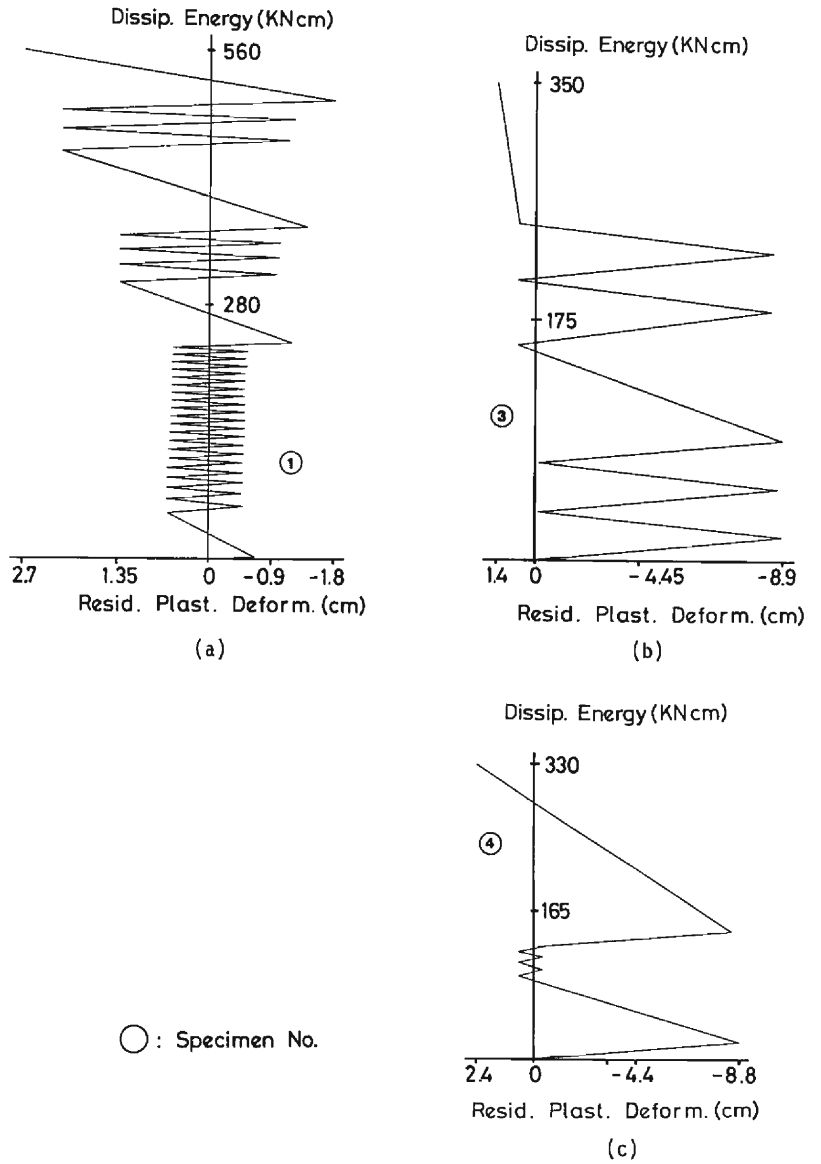

Fig. 7. Residual Plastic Displacement vs. Energy Dissipation of L72-Series.

test specimens, no matter which combination of tensile or compressive loading is applied.

Based on the aforementioned investigations the energy increment or energy rate during each half cycle (see **Fig. 10**, shaded area yields the dissipated energy of half cycle) is calculated as the relation of dissipated energy to the respective plastic deformation ($\bar{\Delta}p_{I,i}$, $\bar{\Delta}p_{D,i}$). The energy rate provides information about the mean value of energy dissipation per unit bending plastification. Since the unit is apparently

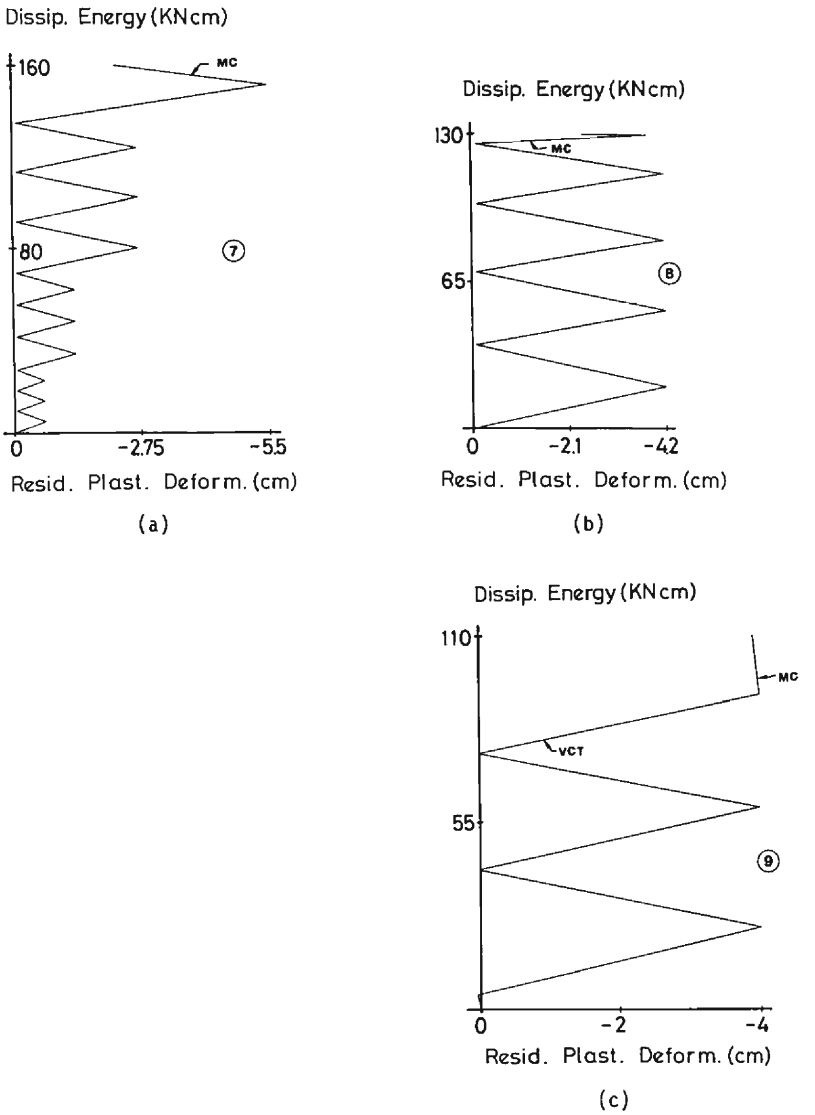

Fig. 8. Residual Plastic Displacement vs. Energy Dissipation of L18-Series.

a strength unit, the energy rate can be looked at as "mean value of strength capacity". Based on the above-mentioned separation between pure tensile plastification and compressive/tensile bending plastification, it seems to be appropriate to perform a normalization by the absolute value of measured buckling load (P_K) for the compressive/tensile bending range. This type of normalization provides the opportunity to compare different types of test specimens under investigation in a somewhat more reasonable way, since it includes effects from the slenderness ratio in terms of P_K. The normalized energy rate, which can be considered the residual proportion of

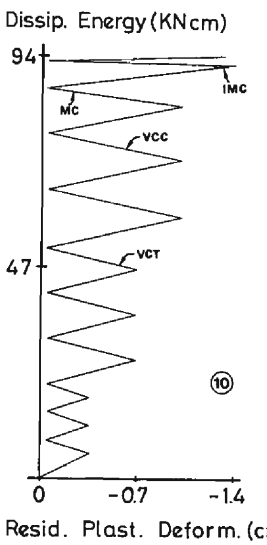

Fig. 9. Residual Plastic Displacement vs. Energy Dissipation of Specimen L09.

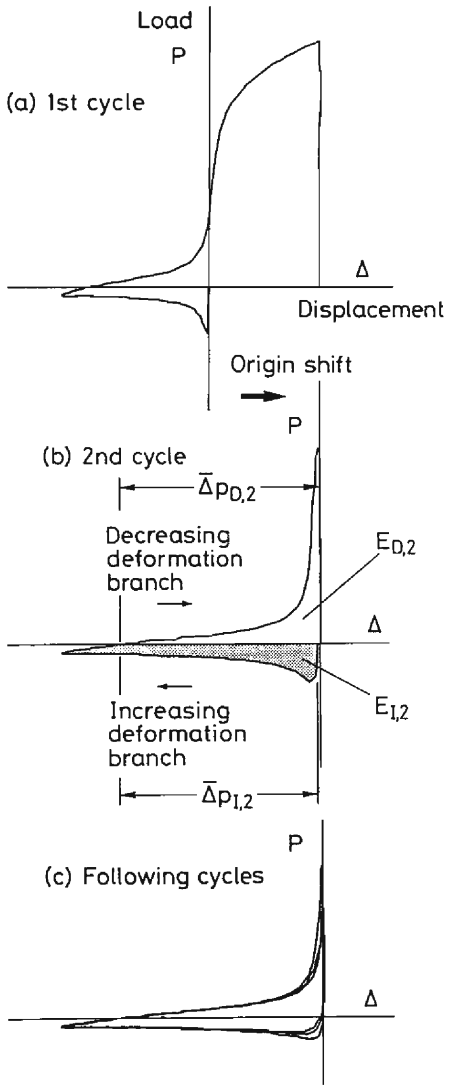

Fig. 10. Schematic Sketch of Energy Separation Approach.

buckling strength, is displayed for all specimens under repeated loading versus number of cycles in **Fig. 11**. In order to provide detailed information about the sensitivity of energy dissipation, increasing and decreasing deformation branches (see **Fig. 10(b)**) have been separated. **Fig. 11** shows that a considerable change in normalized energy rate is either due to increased deformation amplitude or considerable damage. Specimen No. 10 (**Fig. 11(g)**)—where the damage process is rather slow—reveals this fact most clearly. Initial smaller cracks can be noticed at about the 5th (VCT) and 8th (VCC) cycles which obviously have little influence on the normalized energy rate.

However, in the 9th cycle major cracking occurs which is well reflected by a considerable drop in the normalized energy rate. The observed physical damage during testing (indicated in **Fig. 11**) has to be looked at as considerable damage. Only the detected initial cracks (VCT, VCC) provide some information about the intermediate damage range. Comparing the normalized energy rate values when cracks could be observed, it can be seen that visible flexural-tensile cracks (VCT) occur at values about 0.125–0.16, visible flexural-compressive cracks (VCC) at about 0.13 and major cracking at about 0.075–0.10. The values are quite close if one considers that of course some scattering has to be expected.

It should be noted that due to the energy separation, **Figs. 11(a)–(c)** and **Fig. 11(f)** display the normalized energy rate only for the compressive/tensile bending range. The pure tensile deformation induced energy is calculated separately. Of course, there is some effect from tensile plastification on the normalized energy rate in the compressive bending range. This effect can be recognized clearly from **Figs. 11(a)–(c)**. During pure tensile plastification (the first cycle at each amplitude level

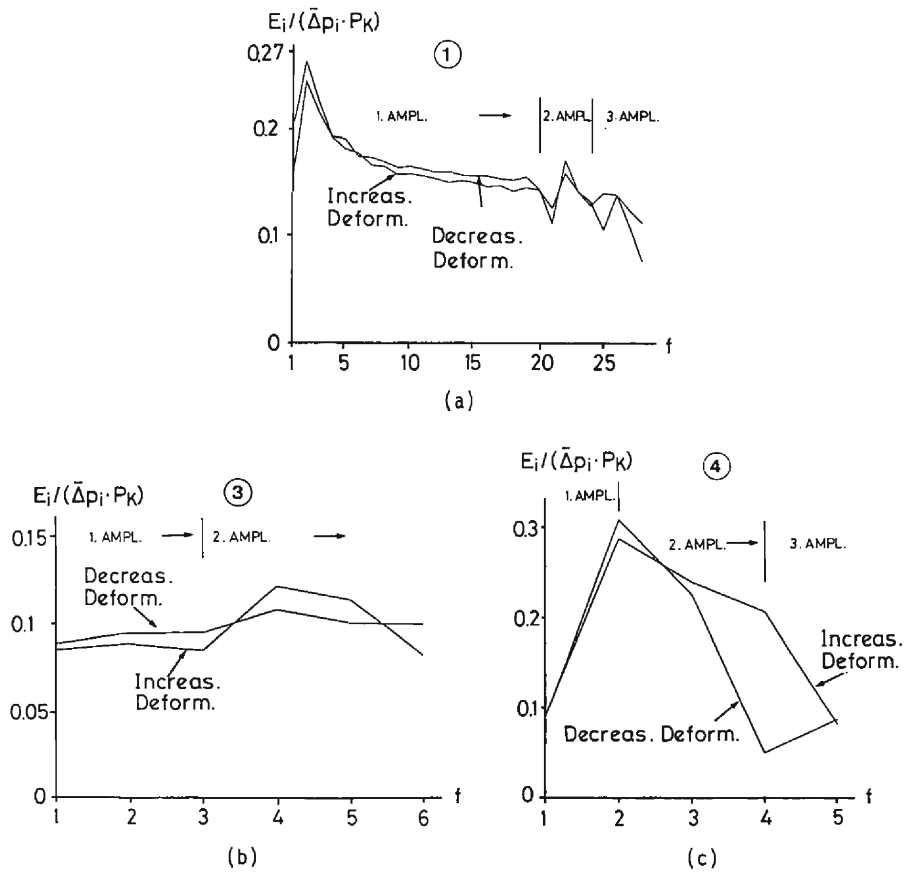

Fig. 11. Normalized Energy vs. Number of Cycles.

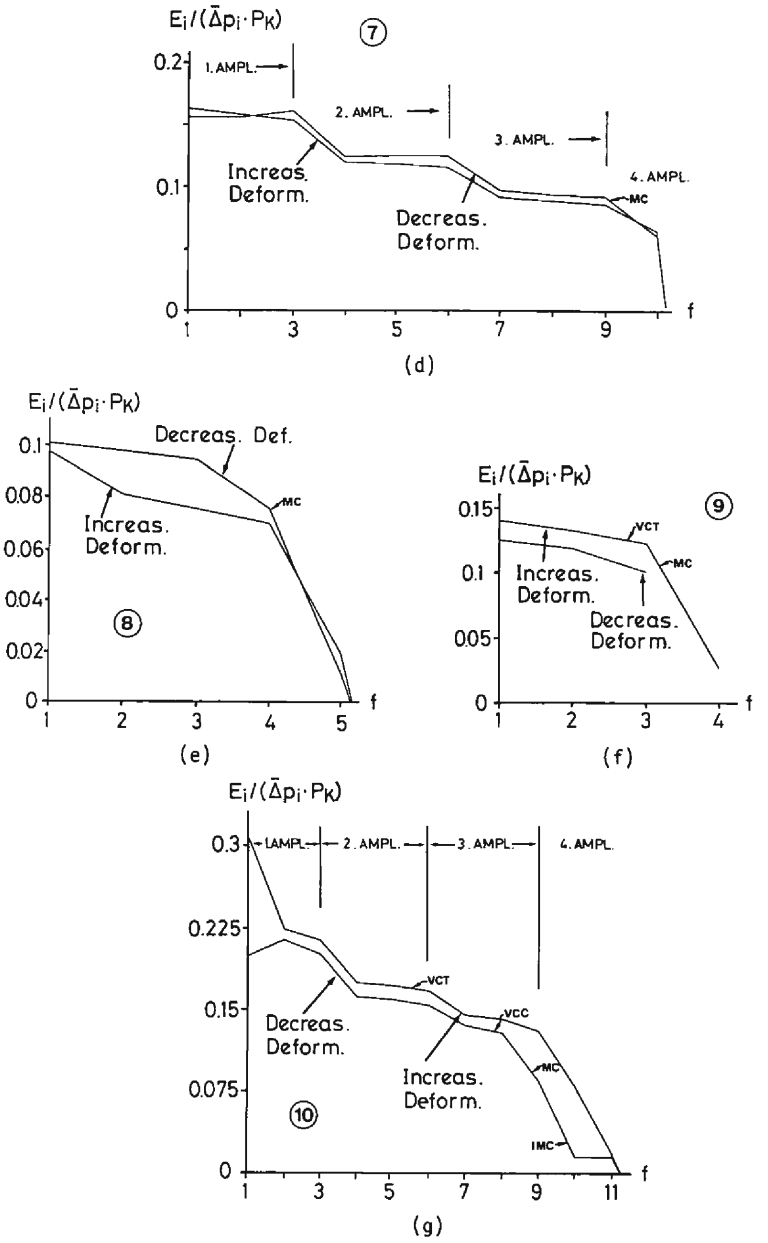

Fig. 11 (continued). Normalized Energy vs. Number of Cycles.

only) the specimen is straightened completely and further hardening takes place. Therefore, some recovery in compressive strength capacity can be observed (see **Fig. 4**), which consequently will yield increased energy rates (**Figs. 11(a)–(c)**). Furthermore, from **Figs. 11(a)–(g)** it can be observed that, in general, the normalized

energy rate of the decreasing deformation branch is slightly larger than the one of the increasing deformation branch. This relation usually changes, in case of considerable damage or pure tensile plastification.

6. Suggested Damage Indicators and a Combination Approach

The investigation so far has been focused on energy contributions, especially on energy contributions due to different types of plastification, e.g. damage processes. It was felt necessary to trace the different energy contributions in order to develop an energy related damage criteria which reflects observed physical damage states. Similar to the energy considerations in the preceding section, damage investigations have to make clear distinctions between different types of failure (failure modes), otherwise misleading conclusions might be drawn. In this investigation, pure tensile failure and compressive/tensile bending failure can be distinguished according to the concept of energy separation suggested in the preceding section. Physically, a damage process has to be considered as a continuous monotonically increasing process. In some cases damage might be considered as 'non-active'—closing of cracks in compression following tensile loading—but in general no damage healing is possible. Damage in this investigation is considered if any part of the cross-section undergoes any degree of plastification. In reality, the observation of physical damage during testing is rather limited, especially in the very low-cycle fatigue range. Visible cracks occur only in case of larger strain values (plastification). Therefore, the observed physical damage quantities related to any kind of damage index have to be considered threshold values for certain damage states.

For the compressive/tensile bending damage process, the use of the normalized energy rate seems to be convenient, since considerable changes of this quantity indicate major damage. In order to enable a reasonable comparison between different types of specimen, a mathematical transformation of physical damage quantities is necessary. The physical based damage quantities usually are transformed to the interval between 0 and 1, where 0 denotes no damage while 1 indicates total damage (complete failure). Any transformation is possible as long as there is no significant physically based contradiction. The energy rate in the preceding section has been normalized by the measured buckling load, since buckling can be considered as basic damage contribution. Thus, the damage indicators for compressive/tensile bending ($D_{CI,i}$ for increasing deformation branch, $D_{CD,i}$ for decreasing deformation branch) can be formulated as:

$$D_{CI,i}=1-(E_{I,i}/(\bar{\Delta}p_{I,i}P_K)) \tag{1a}$$

$$D_{CD,i}=1-(E_{D,i}/(\bar{\Delta}p_{D,i}P_K)) \tag{1b}$$

where i denotes the cycle number, $E_{I,i}$ and $E_{D,i}$ the respective energy dissipation in the i-th cycle (see **Fig. 10**), $\bar{\Delta}p_{I,i}$ and $\bar{\Delta}p_{D,i}$ the plastic deformation quantity related to the deformation branch (**Fig. 10**) and P_K the absolute value of the measured buckling load. In the case of failure, the normalized energy rate is equal to zero, yielding a damage index of 1; for pre-buckling situations, the damage index remains zero.

Since the normalized energy rate decreases sharply after buckling, the suggested damage index will immediately indicate a considerable damage level. This seems to be justified, since from a general engineering design standpoint, buckling is usually considered as considerable damage. Furthermore, the normalizing value is rather easy to estimate, compared to other suggestions[6] in terms of dissipated energy from monotonically compressive tests.

The damage contributions due to pure tensile loading can be easily estimated from the respective energy dissipation as explained in the preceding section. A suitable normalizing value is obtained from monotonic tensile failure tests in terms of the respective energy dissipation. The damage indicator due to pure tensile loading (D_t), therefore, can be written as:

$$D_t=\sum_j E_{t,j}/E_{tu} \tag{2}$$

where $E_{t,j}$ denotes the additional energy dissipation in pure tensile deformation at j-th amplitude level (see **Fig. 12**) and E_{tu} the total energy dissipated in pure tensile monotonic loading to failure. According to the energy separation suggested in the previous section, contributions to D_t will occur only at the first cycle of each amplitude level, in case of further pure tensile plastification. Therefore, D_t remains at constant value as long as the amplitude level of the tensile range is not increased. The summation of $E_{t,j}$ occurs only at the first cycle of increased amplitude in the tensile range.

The suggested damage indicators, of course, are somewhat interdependent. To a certain degree, this is reflected by the dissipated energy contributions (E_i) or energy rate in each cycle, which are conditional energy contributions. Nevertheless for the combination of the damage indicators generally mutual independence is assumed, since little information about the degree of dependency is available or can be modeled on the physical behavior observed so far. A combination of the damage contributions to one damage index (D) is suggested by use of set theory operations; thus

$$D=1-(1-D_{c,i})(1-D_t) \tag{3}$$

where $D_{c,i}$ is taken as the mean of damage contributions from the increasing and decreasing deformation branches in the compressive/tensile bending range, $D_{c,i}=(D_{CI,i}+D_{CD,i})/2$, since damage is calculated if a complete cycle is finished. Investigating Eq. (3) in more detail, it can be observed that the damage index D will yield 1 if any of the involved indicators is equal to 1, which shows consistency with physical behavior, and, therefore, provides justification for the suggested combination model. It might be possible to select a more complicated mathematical combination procedure, but since there seem to be no evidence in a physical sense for the preference of any combination model, Eq. (3) has been selected for reasons of simplicity.

From **Figs. 11(a)** and **(b)**, it was learned that the normalized energy rate is not a monotonically decreasing function; consequently $D_{c,i}$ will not yield monotonically increasing values. In case of small contributions from D_t, therefore, the damage index D, calculated by Eq. (3) will show decreased values within few cycles. This phenomena can be observed after pure tensile plastification which, in general, will

yield strain-hardening effects as long as the strain level is not yet in the descending branch of the monotonic stress-strain curve, and, therefore, the normalized energy dissipation rate in the compressive range shows increased values after only few cycles (see **Fig. 11(a)**). Since damage has to be considered as monotonically increasing even in strain-hardening situations—strain-hardening increases damage because of increased plastification—the contributions for further damage from tensile plastification has to be distinguished with respect to the short time increase of compression induced damage values. Based on the above-mentioned considerations—in order to provide a physically meaningful continuously increasing damage index D—the following procedure is suggested.

$$\tilde{D}_{c,i}=\max\left(D_{c,max},\ D_{c,i}\right) \tag{4}$$

$$D=1-(1-\tilde{D}_{c,i})(1-(D_t-(\tilde{D}_{c,i}-D_{c,i}))) \tag{5}$$

where $D_{c,max}$ denotes the maximum damage indicator of compressive bending range reached so far, i the actual cycle number and $D_{c,i}$ the actual calculated damage contribution of the compressive/tensile bending range. It should be noted that Eq. (5) has to be considered as an extension of the general Eq. (3), in order to ensure con-

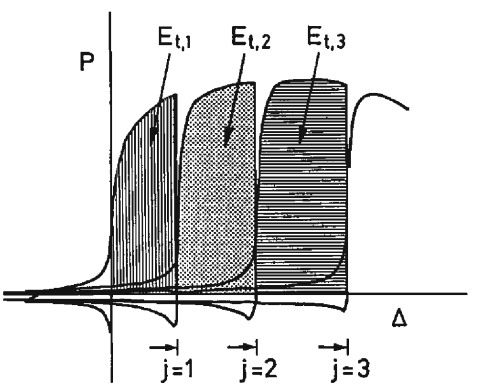

Fig. 12. Definition of Additional $E_{t,j}$ at j-th Amplitude Level.

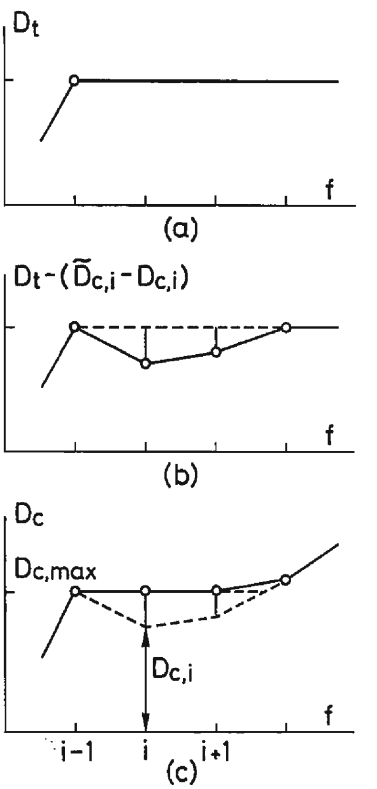

Fig. 13. Schematic Sketch for Combination of Damage Indicators (Eqs. 4 and 5).

tinuously increasing damage values. The formulation of Eq. (5) can be explained as the distribution of damage contributions from pure tensile loading on the subsequent few cycles until the damage contribution from compressive/tensile bending is at the same level as before (see **Fig. 13**). This transformation follows the general physically based assumption of no damage healing. A different justification of Eq. (5) can be given in physical terms. Damage contributions (plastification) from pure tensile loading can be considered as not very localized and somehow spread along the respective specimen, while contributions from compressive/tensile bending seem to be rather localized due to high strain at the critical cross-section caused by a combination of compressive loading and severe bending. If pure tensile plastification occurs, the respective microcracks spread along the specimen will be continuously enlarged to a certain size in the following compressive/tensile bending deformation cycles, which seems to be reflected by continuous increase of residual plastification within compressive range at a constant amplitude level (see **Fig. 7(a)**). One might call this damage process tensile plastification induced damage, since this type of plastification (damage)

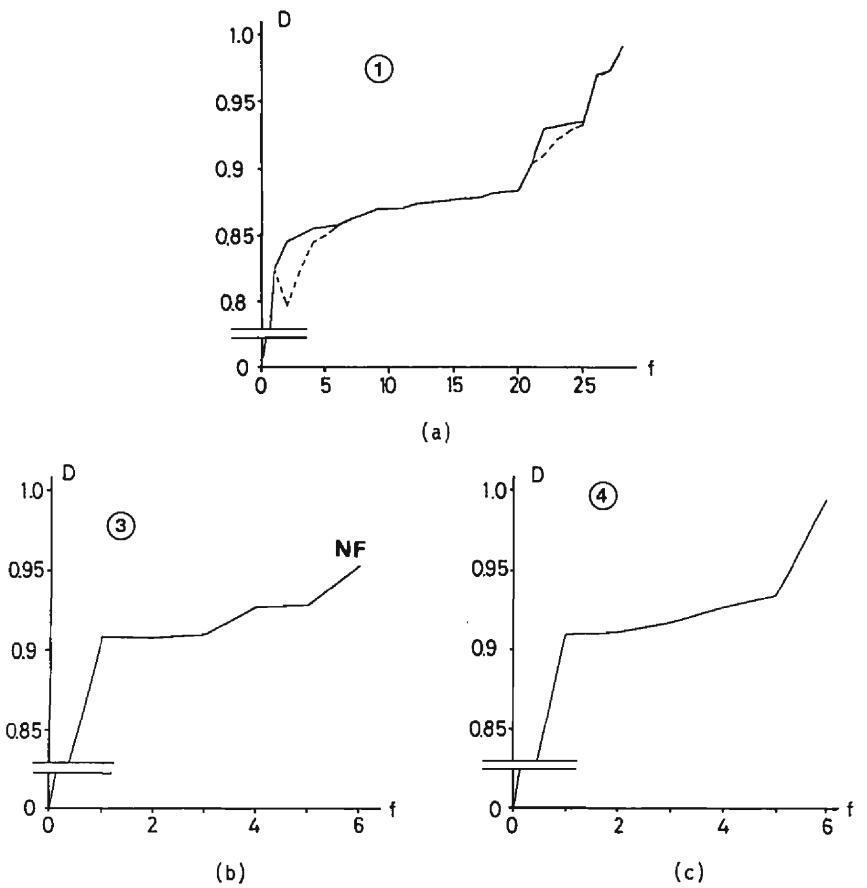

Fig. 14. Damage Development vs. Number of Cycles.

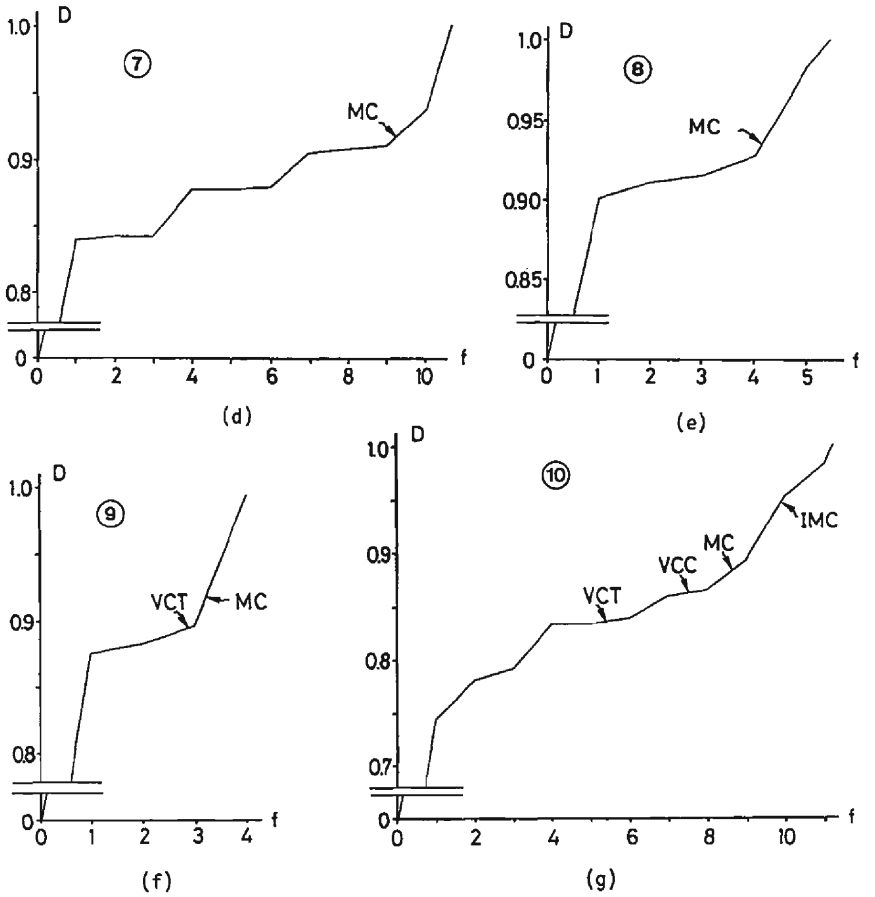

Fig. 14 (continued). Damage Development vs. Number of Cycles.

seems to initiate further compressive/tensile bending damage. It might be worth discussing which one of the suggested indicators should reflect the above-mentioned phenomena. From consistency considerations, preference is given to the separation of tensile damage contributions.

For all tested specimens the suggested damage index is calculated and displayed in **Fig. 14** against number of cycles. Furthermore, the observed physical damage (VCC, VCT, MC, IMC) in the course of testing is indicated at the respective number of cycles. A comparison of calculated damage D applying Eqs. (3) and (5) is given in **Fig. 14(a)**. The solid line is calculated by Eq. (5), while the broken line results from Eq. (3), revealing the effect of separating the tensile damage contributions. Unfortunately, at specimens No. 1, 2 and 4 no physical damage during testing could be detected, but after buckling, a major increase in damage due to tensile plastification was observed. Furthermore, it should be noted that specimen No. 3 did not fail completely, since the loading process was stopped after 6 cycles (small necking had been

noticed) in order to investigate the damage so far achieved by X-ray diffraction methods[1]. A comparison of specimens No. 3 and No. 4 clearly reveal the same degree of damage at the first cycle because of equal load amplitude level. At the 4th cycle, damage in No. 3 is slightly larger, which reflects a larger amplitude in the compressive range. The only difference in the loading patterns of No. 8 and No. 9 is the initial tensile loading in specimen No. 9. Damage occurred after a fewer number of cycles, while major cracking could be calculated at similar damage indices. The difference at first cycle damage was due to pure tensile plastification effects from rather small tensile plastification in specimen No. 9, which is the only cyclically loaded specimen where tensile loading was applied first. Therefore, the various effects from the initial loading direction at the virgin state of the specimen could not be investigated in more detail. Comparison of specimens No. 7 and No. 10 seems to be interesting since both were similar in loading pattern but different in the length of the weak cross-section part. Clearly an increase in damage at enlarged loading amplitude could be observed. Major cracking at No. 7 could be detected at calculated damage of about 0.92, while No. 10 revealed about 0.89 for the same damage pattern. It is felt from this result that a threshold of 0.9 could be established for the occurrence of major cracks, but this has to be verified by further testing results. With respect to earlier damage states the first visible cracks are related to damage values between 0.84 and 0.88 (**Figs. 14(f), (g)**). Due to the scattering of these values and the limited number of physical damage observations these values might provide some information about the expected range of the first visible crack occurrence, but further investigation seems to be necessary to establish a reasonable threshold for this damage state.

7. Conclusions and Further Research

On the basis of experimental investigations using steel plate elements subjected to cyclic axial loading, an energy related damage index is suggested, which would enable damage estimation for complete failure as well as intermediate damage states. The calculated intermediate damage states could be related to observed physical damage in the course of testing. This damage index would consider contributions from expected type of failure modes, as discussed in this investigation: pure tensile and compressive/tensile bending failure. Combinations of different damage contributions (damage indicators) may be performed—in order to provide one damage index—by the application of set theory operations. All damage indicators involved are to be evaluated by the use of the respective normalized dissipated energy or energy rates. A clear distinction in energy contributions could be performed by use of a P-Δ coordinate system whose origin is adaptively shifted, so as to divide the regions of different energy contributions. With respect to observed major cracking, a damage index of about 0.9 appears to be indicative, while first visible cracking could be related to values of the damage index of about 0.84–0.88, but this needs further verification.

With respect to further research, it might be possible to reduce the compressive/tensile bending range to an idealized pure bending state (buckling induced bending).

This approach, which is under investigation, might possibly enable a more sensitive tracing of intermediate damage ranges. Since investigations up to now have been focused on simple cross-sections which in general are elements of members with more complicated cross-sections, future developments will concentrate on structural members of different cross-sectional types. Furthermore, it is felt that information about strain history might enable refinement of the suggested damage model, and, therefore, detailed numerical tracing of the experimental investigations with respect to strain history will be included.

Acknowledgment

The first author gratefully acknowledges the grant awarded to him by the Japan Society for the Promotion of Science (JSPS), which enabled him to perform research at Urban Earthquake Hazard Research Center, DPRI, Kyoto University.

References

1) Iwai, S., U. Bourgund and T. Nonaka: Plastic Fatigue of Structural Members under Repeated Loading—Tests on Failure of Steel Plate Elements, Annuals of Disaster Prevention Research Institute, Kyoto University, No. 32B-1, April 1989, pp. 133–147 (in Japanese).
2) Nonaka, T. and S. Iwai: Failure of Bar Structures under Repeated Loading, Chapter 12 in "Structural Failure", John Wiley & Sons, Inc., 1989, pp. 389–433.
3) Chung, Y. S., C. Meyer and M. Shinozuka: A New Damage Model for Reinforced Concrete Structures, Proc. of 9th World Conference on Earthquake Engineering, August 2–9, 1988, Tokyo–Kyoto, Japan, Vol. VII, pp. 205–210.
4) Kachanov, L. M.: Introduction to Continuum Damage Mechanics, Martinus Nijhof, Dordrecht, Netherlands, 1986.
5) Koenig, G. and A. Oetes: Modeling of Stiffness and Damping Changes in Reinforced Concrete Frames under Seismic Actions, European Earthquake Engineering, No. 1, 1987, pp. 3–10.
6) Meyer, I. F., W. B. Kraetzig and K. Meskouris: Damage in Seismically Loaded Reinforced Concrete Frame Structures—Recent Experiments and Numerical Modeling, Proc. of 9th SMIRT Conference, Vol. H, 1987, pp. 357–362.

Appendix-Notation

The following symbols are used in this paper.

CF =failure in compressive deformation range
$D_{CI,i}$ =damage indicator from compressive increasing deformation branch at i-th cycle
$D_{CD,i}$ =damage indicator from decreasing compressive deformation branch at i-th cycle
D =damage index
$D_{c,i}$ =damage from complete i-th cycle in compressive/tensile bending range
$D_{c,max}$ =maximum damage indicator from compressive bending range reached so far
$\tilde{D}_{c,i}$ =max $(D_{c,max}, D_{c,i})$
D_t =damage indicator due to pure tensile loading
E =energy dissipation
$E_{I,i}$ =energy dissipation (compressive/tensile bending range) at i-th cycle (Increasing Deformation Branch)
$E_{D,i}$ =energy dissipation (compressive/tensile bending range) at i-th cycle (Decreasing Deformation Branch)

$E_{t,j}$ = energy dissipation in pure tensile deformation at j-th amplitude level
E_{tu} = energy dissipated in pure tensile monotonic loading
E_o = maximum strain energy capacity of weak cross-section
f = number of cycles
i = cycle number
IMC = considerable increased major cracking
l = length of weak cross-section
MC = major cracking
P = axial force
P_K = absolute value of measured buckling load
TF = failure due to pure tension
V = mid-height lateral deflection
VCT = visible small cracking at flexural-tension side
VCC = visible small cracking at flexural-compression side
Δ = axial displacement
$\bar{\Delta}_{PI,i}$ = plastic deformation quantity of increasing deformation branch (see **Fig. 10**)
$\bar{\Delta}_{PD,i}$ = plastic deformation quantity of decreasing deformation branch (see **Fig. 10**)